Experimental and numerical investigations on the seismic behavior of bridge piers with vertical unbonded prestressing strands

Zhiguo Sun[1], Dongsheng Wang[2], Kaiming Bi[3] and Bingjun Si[4]

[1]Faculty of Infrastructure Engineering, Dalian University of Technology, Dalian, Liaoning 116024, People's Republic of China. E-mail: szg_1999_1999@163.com.

[2]Faculty of Infrastructure Engineering, Dalian University of Technology, Dalian, Liaoning 116024, People's Republic of China. (Corresponding author). E-mail: dswang@dlmu.edu.cn.

[3]Centre for Infrastructural Monitoring and Protection, School of Civil and Mechanical Engineering, Curtin University, Kent Street, Bentley, WA 6102, Australia. E-mail: kaiming.bi@curtin.edu.au.

[4]Faculty of Infrastructure Engineering, Dalian University of Technology, Dalian, Liaoning 116024, People's Republic of China. E-mail: sibingjun@sina.com.

Abstract

In the performance-based seismic bridge design, piers are expected to undergo large inelastic deformations during severe earthquakes, which in turn can result in large residual drift and concrete crack in the bridge piers. In this paper, longitudinal unbonded prestressing strands are used to minimize residual drift and residual concrete crack width in reinforced concrete (RC) bridge piers. Seven pier specimens were designed and tested quasi-statically and the numerical simulations were carried out. The effectiveness of using vertical unbonded prestressing strands to mitigate the residual drift and concrete crack width of RC bridge piers are examined and discussed in detail. It is found that the residual drift and residual concrete crack width of the piers can be reduced significantly by using the prestressing strands. Moreover, the strands can increase the lateral strength of the piers while have little influence on the ductility capacity of the piers. The hysteretic

curves, residual drifts and strand stress of the piers predicted by the numerical model agree well with the testing data and can be used to assess the cyclic behavior of the piers.

Keywords Seismic design of bridges piers, Unbonded prestressing strands, Residual drift, Residual concrete crack width, Quasi-static test, Numerical simulation

1 Introduction

Bridges are key components in the transportation network, they can provide immediate emergency services following an earthquake. It is of particular importance to ensure the seismic safety of bridge structures during severe earthquakes. In the performance-based seismic design of bridge structures, bridge piers are expected to undergo large inelastic deformations during severe earthquakes, which in turn can result in large residual displacement and concrete crack width and lead to malfunction of the bridge structures. For example, following the 1995 Kobe earthquake, many reinforced concrete (RC) bridge piers with a residual drift ratio (pier residual lateral displacement divided by the pier height) larger than 1.75% were demolished in spite of the apparent light damage (Fujino et al. 2005; Kawashima et al. 1998). During the 2008 Wenchuan earthquake, the maximum residual concrete crack width in the No. 5 pier of the Miaoziping bridge reached as much as 0.8 mm. With such a wide crack, the piers under the water have to be retrofitted to protect them from corrosion attack. The cost of retrofitting was significantly high due to underwater construction of the concrete (Zhuang et al. 2009). Recently, a growing number of high speed railway bridges and cross sea bridges are designed and constructed in China. In the seismic design of high speed railway bridges, it is especially important to reduce the residual drift of the piers to ensure the safety and stability of the high speed trains. On the other hand, concrete cracking can

seriously threaten the long-term durability of the cross sea bridge piers, which should be adequately considered in seismic design of these piers (Guo et al. 2015; Moshref et al. 2015).

To minimize the residual drift in bridge piers, a new pier design concept by using longitudinal prestressing strands was proposed. For example, Zatar and Mutsuyoshi (2002) suggested using partially prestressed concrete for the bridge piers and a series of quasi-static and pseudo-dynamic tests were carried out to examine its efficiency. It was found that employing prestressing strands in RC bridge piers could result in substantial reductions of residual drift after an earthquake. Sakai and Mahin (2004a, 2004b) proposed a similar design to minimize residual drift of RC bridge piers by using longitudinal prestressing strands to replace some of common longitudinal mild bars. The seismic behavior of such prestressed piers was investigated through a series of quasi-static and dynamic analyses. Moreover, a series of earthquake simulator tests were conducted to validate the effectiveness of using prestressing strands in mitigating the residual drift of the piers (Mahin et al. 2006). The Unbonded Bar Reinforced Concrete (UBRC) structure, which consists of a conventional RC structure and vertical unbonded prestressing bars, was proposed by Iemura et al. (2004). To evaluate the seismic behavior of the UBRC structures, cyclic loading and pseudo-dynamic tests for pier specimens were carried out. It was found that UBRC piers exhibit stable seismic response even under strong earthquakes and the residual drift was small. In recent years, a new design concept of segmental precast concrete bridge pier was proposed to accelerate bridge construction (Shim et al. 2008; Wang et al. 2008; Yamashita and Sanders, 2009; Ou et al. 2010), in which the unbonded prestressing strands were used to hold the pier segments together and bring the piers back to their original position under lateral loads.

According to the previous studies, it is clear that the residual drift of bridge piers can be decreased evidently by employing longitudinal unbonded prestressing strands. It should be noted that the residual crack width of the piers will be restricted as well as a result of the restoring force provided

by the prestressing strands. Thus, the use of prestressing strands would bring great benefit for the seismic design of the bridge piers in view of mitigating residual drift and concrete crack width.

Until recently, studies on the seismic behavior of cast in place bridge piers with longitudinal unbonded strands are limited, and most of previous studies focused on the residual drift. Very little effort has been devoted to study the residual concrete crack widths of the piers after an earthquake, which is especially important for the long-term durability of the piers. In this study, the longitudinal unbonded prestressing strands are used to minimize residual drift and residual concrete crack width in RC bridge piers. Both experimental and numerical investigations are carried out to investigate the seismic behavior of the proposed bridge piers. Seven pier specimens were designed and tested quasi-statically to evaluate the effect of the prestressing strands on mitigation the residual drift and residual concrete crack width of the piers after an earthquake. The influences of various parameters including the prestressing force ratio, the mechanical prestressing ratio and the location of the prestressing strands, on the residual drift and residual concrete crack width, were experimentally investigated. Finally, a finite element (FE) model was developed and calibrated by using the open-source finite element code OpenSees (Mazzoni et al. 2007) based on the testing data.

2 Experimental program

2.1 Test specimens

To experimentally evaluate the seismic behavior of the RC bridge piers with vertical unbonded strands under cyclic loading, seven 1:4 scaled pier specimens with a cantilever scheme were designed and tested. Fig. 1 and Table 1 show the design details of the pier specimens. All the specimens had a circular section with a diameter of 300 mm and with a heavy RC footing. As shown in Fig. 1(a), the height of the specimens measured from the top surface of the footing to the

96 point where lateral loading was applied was 1100 mm, corresponding to an aspect ratio of 3.67,
97 which normally leads to flexural failure of the specimens (Hashimoto et al. 2005; Sun et al. 2012).
98 Fig. 1(b) summarizes the reinforcement layout. As shown in Fig. 1(b)-1, specimen RC-1
99 represented a conventional RC bridge pier without prestressing strands. This specimen was used as
100 a reference for comparison with results obtained from specimens with prestressing strands. This
101 specimen was reinforced with eight 12 mm-diameter longitudinal mild bars evenly distributed
102 around the perimeter. Mild bars of 8 mm in diameter were used as transverse reinforcement and
103 spaced at a distance of 75 mm along the pier height, resulting in a transverse reinforcement ratio of
104 1%.
105 Specimen PRC-1 was a standard specimen with prestressing strands. This specimen was designed
106 to be the same as specimen RC-1 except that prestressing strands were included. Four 12.7
107 mm-diameter unbonded strands (each strand with a nominal area of 98.7 mm^2) were used with a
108 total prestressing force ratio of 0.1 (the definition of prestressing force ratio ζ can be found in
109 Equation (3)). The strands were arranged in a square pattern with a side length of 135 mm. Fig.
110 1(b)-2 shows the reinforcement layout of specimen PRC-1. Specimen PRC-2 was designed the
111 same as specimen PRC-1 except for the longitudinal mild bars, where as shown in Fig. 1(b)-3, eight
112 8 mm-diameter longitudinal mild bars were used in this specimen to evaluate the longitudinal mild
113 bars on the seismic behavior of the piers with prestressing strands. Specimen PRC-3 (Fig. 1(b)-4)
114 was design to evaluate the amount of prestressing strands on the behavior of the piers. Only two
115 strands were used in this specimen, and other parameters were the same as specimen PRC-1.
116 Specimen PRC-4 and Specimen PRC-5 were designed to evaluate the initial prestressing stress on
117 the behavior of the piers. In specimen PRC-4, the prestressing force ratio was reduced to 0.05, while
118 in specimen PRC-5, it reached 0.15. For the reinforcement layouts of specimens PRC-4 and PRC-5,
119 they were exactly the same as specimen PRC-1. Specimen PRC-6 was designed with four
120 prestressing strands concentrated at the center of the section to evaluate the arrangement of the

strands on the behavior of the piers, as shown in Fig. 1(b)-5. Thus totally three different types of prestressing strand layout are considered in the test and they are summarized in Fig. 1(c). It should be noted that, the prestressing strands were arranged inside the mild longitudinal bars, and the concrete cover depth of the prestressing strands was much larger than the mild longitudinal bars. As a result, the strands would be safe enough against corrosion damage compared with mild longitudinal bars.

Before the tests, all the important parameters related to the specimens were tested and measured. For example, the average concrete compression strength was measured as 55.9 MPa by using 150×150×150 mm cubic specimens. The yielding strengths of the 8 mm-diameter and 12 mm-diameter mild bars were 517 and 453 MPa, respectively. And the ultimate strengths of the 8 mm-diameter and 12 mm-diameter mild bars were 611 and 634 MPa, respectively. The ultimate strength of the 12.7 mm-diameter prestressing strand was 1939 MPa. All these parameters were adopted in the numerical simulations in Section 4.

To facilitate further explanation, the following parameters are defined in the present study. They are: the total axial force ratio n, axial load ratio η, prestressing force ratio ζ and mechanical prestressing ratio λ. The parameters are defined as follows:

$$n = \frac{N + N_p}{f_c^{'} A} \tag{1}$$

$$\eta = \frac{N}{f_c^{'} A} \tag{2}$$

$$\zeta = \frac{N_p}{f_c^{'} A} \tag{3}$$

$$\lambda = \frac{f_{py} A_p}{f_{py} A_p + f_y A_s} \tag{4}$$

where N is the applied axial load, N_p is the total prestressing force before test, f_c' is the cylinder concrete compressive strength, A is area of the cross section, A_p and f_{py} are the area and yielding stress (defined by the 85% of its ultimate strength) of the prestressing strands in the cross section and A_s and f_y are the area and yielding stress of mild longitudinal bars. Obviously, the parameters η and ζ representing the axial loads induced by the weight of the bridge superstructure and the prestressing strands, respectively. The parameter λ accounts for the contribution of the prestressing strands to the overall cross-sectional capacity of the pier. Table 1 summarizes the corresponding values for different specimens.

2.2 Test setup and loading sequence

The specimens were tested under lateral cyclic loadings while simultaneously being subjected to a constant axial load. The test setup for each of the specimen is shown in Fig. 2, the specimen was vertically fixed to the laboratory floor and the top of the pier was held by a vertical hydraulic actuator to provide axial load, which was used to simulate the weight of the bridge superstructure. Under the vertical actuator, the specimen was loaded by two horizontal actuators (actuator A and actuator B) to provide the lateral cyclic loads. It should be noted that as the horizontal actuators could only provide compressive force, but not able to provide tensile force, two horizontal actuators were placed in a straight line to provide the lateral cyclic loads. During the tests, actuator A was first used to push the specimen to a predefined positive displacement, while actuator B was separated from the specimen. Then, actuator B was used to push the specimen to a predefined negative displacement, and actuator A was separated from the specimen. By using this method, the cyclic loadings were achieved. The lateral loading history was divided into two phases: the load control phase and the displacement control phase. The load control phase was used to determine the specimen's experimental concrete cracking strength $F_{cr,e}$. Then, the specimens were tested under displacement control mode to study the inelastic behavior of the specimens. During the load control phase, the theoretical concrete cracking strength $F_{cr,t}$ was first calculated by using the software

Response-2000 (Bentz 2000), which is based on the Modified Compression Field Theory (Bentz et al. 2006). Then, lateral loads corresponding to 0.6, 0.8, 1.0, 1.2, and 1.4 times of $F_{cr,t}$ were applied to the specimens, with each load repeated twice. During the displacement control phase, tests were conducted to drift levels of 0.32%, 0.5%, 1.0%, 1.5%, 2.0%, 2.5%, 3.0%……, each cycle was repeated three times, until the lateral strength of the pier declined to 85% of the peak load. Figure 3 shows the lateral loading histories. It should be noted that drift ratio was used as a dimensionless measure of pier top displacement in the present study. It was defined for the test specimens as the lateral displacement at the loading point divided by the height of the specimen. The horizontal load was measured by two load cells on the horizontal actuators, and the horizontal top displacement was measured by a displacement transducer. This transducer was fixed to the laboratory floor to obtain the pier top displacement. For specimen with prestressing strands, force measuring transducers were used to measure the stress of the prestressing strands when the specimen was loaded to the maximum displacement during the first cycle at each load or displacement level. For specimen PRC-6, only one force measuring transducer was used to measure the total stress of all strands. For other specimens, each strand was equipped with a transducer to measure the stress separately. During the tests, the concrete crack width was measured using the DJCK-2 Crevice Width Finder (with an accuracy of 0.01 mm), which was manufactured by the Beijing Earth Long Science and Technology Co., Ltd. It should be noted that, both the maximum and residual concrete crack widths were measured in the present study. The maximum crack width was measured when the specimen reached a maximum top displacement (in the first cycle at each load or displacement level). And the residual crack width was measured when the specimen was unloaded (zero lateral load, in the first cycle at each load or displacement cycle). Both the maximum and residual crack width listed in the current study was the measured maximum value for each specimen.

3 Experimental results

3.1 Damage pattern and hysteretic response of the specimens

During the tests, no obvious difference is observed for the damage development and failure pattern between the specimens with and without prestressing strands. For illustration purpose, Fig. 4(a) shows the failure pattern of the pier without prestressing strands (specimen RC-1) and the failure pattern of specimen PRC-1 is plotted in Fig. 4(b) to represent the pier with prestressing strands. It can be seen that both the specimens show a flexural failure mode in regions close to the bottom of the specimens (the plastic hinge regions).

The damage developments of all the specimens are similar with each other as well. During the load control phase, horizontal flexural cracks develop first in the plastic hinge regions and the crack length and width increase with the top load. The measured maximum crack width reaches 0.09 mm in specimen RC-1, while in other specimens they are between 0.03-0.06 mm. Table 2 lists both the experimental and theoretical concrete cracking strengths of the specimens, it could be found that all the specimens with prestressing strands show a higher concrete cracking strength than specimen RC-1, indicating that the concrete cracking strength of the pier could be increased by using vertical prestressing strands. The experimental and theoretical concrete cracking strengths are close with each other, and the experimental concrete cracking strengths of the specimens are between 0.8 and 1.2 times of the theoretical concrete cracking strengths. For the residual crack, the measured residual width is about 0.01 mm in specimen RC-1. While in other specimens (in which prestressing is applied), no obvious residual crack is observed when the specimens unloaded from the maximum lateral load during the load control phase.

During the displacement control phase, the residual cracks are observed in all the specimens and both the maximum and residual crack widths increase with the increment of drift ratio. At the drift level of 0.32% (3.5mm), the maximum crack width reaches 0.25 mm in specimen RC-1, while in other specimens they are not larger than 0.15 mm. The residual crack width is 0.02 mm in specimen RC-1 while it is 0.01 mm in other specimens. At the drift level of 1% (11 mm), the maximum crack

width is 0.9 mm in specimen RC-1 while the widths are between 0.5-0.7 mm in other specimens. For the 2% drift level (22 mm), the spalling of the concrete cover initiates in all the specimens, and the specimens reach the maximum lateral load capacity.

It should be noted that during the displacement control phase, some horizontal flexural cracks extend to the regions which are close to the neutral axial of the cross section. Within this region, the absolute value of the normal stress is much smaller than the shear stress, some flexural cracks change to be diagonal shear cracks, as shown in Fig. 4(c). However, generally speaking the performance of all the specimens is dominated by concrete spalling and longitudinal bar buckling damages, which could be classified as flexural failure mode.

At the later stages of loading (where drift levels are larger than 2%), the cover concrete peels off and the spiral and longitudinal bars are exposed (Fig. 4(d)), longitudinal bar buckling and concrete core crushing (Fig. 4(e)) follow progressively within the next displacement cycles. At the end of the test, the concrete spalling heights of all the specimens are measured and illustrated in Fig. 5, it can be seen that the concrete spalling damages of all the specimens are concentrated at the plastic hinge regions, the spalling heights are between 210 and 330 mm, corresponding to 0.7-1.1 times of the section depth. Except specimen PRC-4, all the specimens with prestressing strands show larger or similar spalling heights compared with specimen RC-1.

It should be mentioned that during the test of specimen PRC-2, one prestressing strand fails due to the damage of the anchorage and a snapping noise is heard when the drift level reaches 0.5%. For all the other specimens, the prestressing strands perform well and no rupture damage is observed during the tests.

Figure 6 shows the lateral load vs displacement (drift) hysteretic curves for all the specimens, in which the occurrences of concrete cover spalling, longitudinal bar buckling and prestressing strand failure damage are indicated. It can be seen from these figures that a fat hysteretic curve with no pinching effect is observed for specimen RC-1, in which no prestressing strand is used. For

specimens with prestressing strands, specimens PRC-3 and PRC-4 display a slight pinching effect while pinching is evident in other specimens, and specimen PRC-2 shows the most obvious pinching effect among all the specimens. Obviously, the pinching effect is attributed to the restoring force (prestressing force) provided by the prestressing strands. It should be noted, specimen PRC-2 is designed with the maximum mechanical prestressing ratio (λ=0.76) while the ratio in specimen PRC-3 is the minimum (λ=0.44). Even after one prestressing strand is failed, the mechanical prestressing ratio (λ=0.70) in specimen PRC-2 is the largest one among all the specimens, indicating that a high mechanical prestressing ratio will lead to significant pinching effect of the piers. The fat hysteretic curve of specimen PRC-4 would attribute to the low prestressing stress of the strands in larger lateral displacement, which would be illustrated in the following section of the work.

3.2 The strand stress

The strand stress is recorded at the maximum displacement during the first cycle at each displacement level. Figure 7 shows the measured strand stress under different drift ratios. It should be noted that as only one force measuring transducer is used, the values in specimen PRC-6 representing the average ones of all the four strands. It could be found that the strand stress would be increased or decreased as a result of the lateral displacement. It also can be seen from the figure that the stress-drift relationship could almost be regarded as linear in both the positive or negative directions.

Table 3 tabulates the strand stress values in all the specimens. It includes the initial strand stress $\sigma_{PS,1}$ of all the strands in each specimen measured after the axial load is applied, the measured maximum strand stress $\sigma_{PS,max}$ and the minimum strand stress $\sigma_{PS,min}$ of the strands, and the stress change amplitude $\sigma_{PS,var}$ of each strand during the tests. It could be found that except strand PS3 in specimen PRC-2 (failed due to damage of the anchorage), the measured maximum strand stress is 1410 MPa (strand PS3 in specimen PRC-5), it is about 73% of the ultimate strength of the strand (1939 MPa as mentioned in Section 2.1), the strands would be elastic and no yielding or rupturing

damage would be observed. The measured minimum strand stress is only 8 MPa for strand PS1 in specimen PRC-4, and the minimum stress of other strands in specimen PRC-4 are less than 200 MPa.

The relationship between the total prestressing force provided by the strands (recorded at the maximum displacement during the first cycle at each displacement level) and the top drift ratio of the specimens is shown in Fig. 8. Obviously, specimen PRC-5 has the largest prestressing force while the force in specimen PRC-4 is the minimum. Except specimen PRC-2, the total prestressing force in all the specimens increases gradually with the lateral drift. For specimen PRC-2, the total prestressing force decreases suddenly at a drift ratio of 0.5% as a result of the failed strand.

3.3 Residual drifts

Residual drift is an important measurement of post-earthquake functionality of a bridge, normally it is used to determine whether or not a bridge remains functional following an earthquake. During the tests, the residual drifts of the specimens are measured when the lateral loads reached zero during the first cycle at each displacement level. Figure 9(a) shows the relationship between the residual drift ratio and the applied drift ratio for each specimen, and they are compared in different groups from Figs. 9(b) to 9(f) to make them clearer.

It is obvious that the residual drift in specimen RC-1 is higher than all of the other specimens when the same drift level is considered, which indicates that employing prestressing strands is quite effective in reducing the residual drift of bridge piers. It also can be seen from the figure that among all the specimens with prestressing strands, specimen PRC-4 exhibits the largest residual drift, while specimen PRC-2 has the minimum residual drift. Except specimen PRC-4, the residual drift in specimen PRC-3 is much larger than other specimens with prestressing strands in the positive direction. While in the negative direction, the residual drift of specimen PRC-3 is larger than specimens PRC-2 and PRC-6. This is because, as can be seen from Table 1, the mechanical prestressing ratio λ in specimen PRC-2 is the largest (0.76 before the test and changed to 0.70 after

one prestressing strand failed) among all the tested specimens. While for specimen PRC-3, the mechanical prestressing ratio is the minimum (0.44), which indicates that larger mechanical prestressing ratio can result in lesser residual drift. The reason for the larger residual drift in specimen PRC-4 is attributed to the low prestressing stresses in the strands, as illustrated in the above section.

Specimen PRC-2 is designed with less longitudinal mild bars than specimen PRC-1, and the mechanical prestressing ratio of specimen PRC-2 (λ=0.76 before the test and changes to 0.70 after one prestressing strand failed) is larger than specimen PRC-1 (λ=0.61). As a result, there is a reduction in residual drift ratio, as shown in Fig. 9(b). The amount of prestressing strands in specimen PRC-3 is reduced compared with specimen PRC-1, which results in a low mechanical prestressing ratio (λ=0.44 for specimen PRC-3). The reduction of the prestressing strands leads to higher residual drift ratios, as shown in Fig. 9(c). From the above analysis, it is clear that the mechanical prestressing ratio λ is an important parameter for controlling the residual drift of the pier, larger mechanical prestressing ratio can result in lesser residual drift in the piers.

The initial prestressing stresses are changed in specimens PRC-4 and PRC-5, and the effect of the initial prestressing stress on the residual drift is shown in Figs. 9(d) and 9(e). It can be found that specimen PRC-4 exhibits notable larger residual drift ratio than PRC-1. While the residual drift ratio in specimen PRC-5 is slightly larger than that in PRC-1. These results indicate that the influence of the initial prestressing stress on the residual drift is not clear. It should be noted that the prestressing stress for strand PS1 in specimen PRC-4 is reduced to 8 MPa in large lateral displacement, the restoring force (prestressing force) provided by this strand would be neglected, which would induce larger residual drift in specimen PRC-4. From the above analysis, it could be concluded that the initial prestressing stress should have little influence on residual drift of the pier if the strands are effective under seismic action.

315 The residual drift in specimen PRC-6 is almost identical to PRC-1, as shown in Fig. 9(f). This is
316 because both the specimens are designed with the same mechanical prestressing ratio (λ=0.61). Also,
317 the total prestressing forces in specimens PRC-1 and PRC-6 are almost the same during the tests, as
318 shown in Fig. 8. In that case, the location of the prestressing strands has little influence on the
319 residual drift of the piers.

320 3.4 Residual crack width

321 Residual concrete crack width is also important for the usability of the pier following an earthquake.
322 Figure 10(a) shows the relationship between the measured maximum residual crack width and
323 lateral load for all the specimens, and they are compared in different groups from Figs. 10(b) to 10(f)
324 to make them clearer. It should be noted that as large residual crack width will lead to corrosion
325 damage of the reinforcement and deterioration of the bridge piers. Normally it is required to limit
326 the residual crack width within 0.2 mm, beyond this value, corrosion of the reinforcement and
327 concrete cover spalling damage would occur. It is thus believed that the controlling of residual
328 crack width becomes meaningless if it is larger than 0.2 mm. In Figs. 10(b) to 10(f), the y-axis is
329 thus only up to 0.2 mm. The measured residual crack width beyond 0.2 mm can be found in Fig.
330 10(a).
331 It can be seen from Fig. 10(a) that the residual crack widths in specimen without prestressing
332 strands (RC-1) are much larger compared with the specimens with prestressing strands. The
333 maximum residual crack width reaches as much as 1.0 mm in specimen RC-1, while they are not
334 larger than 0.4 mm in all the other specimens.
335 In all the specimens with prestressing strands, the residual crack widths in specimen PRC-4 are
336 much larger than the other specimens. And specimen PRC-5 has the minimum residual crack width
337 compared with other specimens. This is because, as can be seen from Table 1, the prestressing force
338 ratio in specimen PRC-5 is the largest (ζ=0.15) among all the tested specimens while for specimen
339 PRC-4 it reaches the minimum (ζ=0.05), which indicates that the prestressing force ratio has a

significant influence on the residual crack width, larger prestressing force ratio can result in smaller residual crack width.

Specimen PRC-2 is designed the same as specimen PRC-1 except for longitudinal mild bars, and the mechanical prestressing ratio of specimen PRC-2 (λ=0.76 or 0.70) is larger than specimen PRC-1 (λ=0.61). As a result, the residual crack width in specimen PRC-2 is much smaller than specimen PRC-1, as shown in Fig. 10(b). Also, the residual crack width in specimen PRC-3 (λ=0.44) is larger than specimen PRC-1 (λ=0.61), as shown in Fig. 10(c). Indicating that larger mechanical prestressing ratio will lead to smaller residual crack width.

As shown in Fig. 10(f), the residual crack widths in specimens PRC-1 and PRC-6 are almost similar with each other. These observations indicate that the arrangement of the strands has little influence on the residual crack width of the piers if both the prestressing force ratio and the mechanical prestressing ratio of the specimens are identical with each other.

As mentioned above, both the residual drift and residual crack width of specimen PRC-4 are larger than other specimens with prestressing strands, indicating that the strand stress has a significant influence on the residual drift and residual crack width. To minimize the residual drift and concrete crack width in bridge piers, the strand should be kept effective under seismic actions.

3.5 Strength and ductility of the specimens

The strength and ductility of the specimens are compared with each other in this section. The associated parameters, including the peak load $F_{\max}$, yield displacement Δ_1, ultimate displacement Δ_μ, displacement ductility factor μ_Δ, and ultimate drift ratio R, are obtained based on the skeleton curve of the specimens as described in Fig. 11. The parameters are defined by the following equations:

$$F_{\max} = \frac{F_{\max}^{+} + F_{\max}^{-}}{2} \tag{5}$$

$$\Delta_1 = \frac{\Delta_1^+ + \Delta_1^-}{2} \tag{6}$$

$$\Delta_\mu = \frac{\Delta_\mu^+ + \Delta_\mu^-}{2} \tag{7}$$

$$\mu_\Delta = \frac{\Delta_\mu}{\Delta_1} \tag{8}$$

$$R = \frac{\Delta_\mu}{L} \tag{9}$$

where L is the height of the specimen, the superscripts + and – denote the corresponding values obtained at the positive and negative phases respectively.

Table 4 lists the measured and calculated strength and ductility parameters of all the specimens. It is shown that the peak loads of all the specimens with prestressing strands are higher than specimen RC-1, indicating an increasing of the lateral strength of the pier specimens by using unbonded prestressing strands. As for the ductility parameters Δ_μ, μ_Δ and R, it could be found that all the specimens exhibit good ductility. The displacement ductility factors of all the specimens are larger than 4.0, and the ultimate drifts of all the specimens are larger than 3.0%, except for specimen PRC-2. Also should be noted, the ductility of the specimens with prestressing strands are essentially the same with specimen RC-1, indicating no obvious change of ductility capacity by using prestressing strands. This is because, as shown in Table 1, the axial load ratio η of all the specimens is only 0.10, and the total axial force ratio of all the specimens is equal or less than 0.25, which is much lower than the axial loading capacity of the piers. With such a low axial load ratio, the using of the vertical prestressing strands will not have an obvious influence on the deformation capacity of the piers. In most cases, the axial load ratio of the commonly used bridge piers under dead load would be less than 0.1, so it is practical to reduce the seismic residual drift and residual concrete crack width of these piers by using vertical prestressing strands.

4 Numerical simulations of the tests

Experimental studies are expensive, time consuming, labor extensive and sometimes may be limited by the capacities of the experimental facilities. In contrast, numerical simulations are more convenient and efficient for the analysis. A reliable finite element model is believed to be necessary for the readers to appreciate the results of the paper. In the present study, numerical simulations are also carried out by using the open-source finite element code OpenSees. The numerical results are compared with the experimental data.

4.1 Description of the numerical model

The total lateral deformation of a column subjected to lateral loads is comprised of deformations due to three response mechanisms: flexure, longitudinal bar slip at the column footing, and shear. In the numerical simulation, each deformation component can be conveniently modeled (Yavari et al. 2009; Shoraka et al. 2013). However, as all the specimens failed in flexural mode in the present study, the shear deformation of the specimen is neglected in the numerical model.

The specimens are modeled by using the open-source finite element code OpenSees (Mazzoni et al. 2007) and the finite element scheme is illustrated in Fig. 12. Owing to the large size of the RC footing, it is not modeled and only the specimen above the footing top is considered. Also should be noted, as the prestressing strands are anchored at the bottom of the footing, the strand length is larger than the specimen height in the numerical model.

The total lateral response of the specimen are modeled by coupling flexure and longitudinal bar slip responses by two elements in series, where the force in each element is the same and the total deformation is the sum of individual element deformations. Flexural deformation is modeled by the nonlinear beam-column element, while the longitudinal bar slip deformation is modeled by the zero-length fiber section element. As shown in Fig. 12, each specimen consists of a single nonlinear beam-column element and a zero length fiber section element located at the bottom of the

beam-column element. The length of the beam-column element (distance between Node 2 and Node 3) is the same as the height the specimen between footing top surface to the point where lateral loading is applied. The fiber section element is defined by two nodes (Node 1 and Node 2) at the same location.

4.1.1 Flexural deformation

The force-based nonlinear beam-column element, implemented in OpenSees, accounts for the nonlinear flexural deformation by assuming plane sections remain plane and captures the spread of plasticity along the element while the shear and longitudinal bar slip deformations are neglected (Spacone et al. 1996a, 1996b). The nonlinear hysteretic behavior of the element derives from the constitutive relations of concrete and reinforcing steel fibers into which each section is divided. All concrete fibers are modeled by using the “Concrete01” uniaxial material model in OpenSees, which is based on the modified Kent and Park concrete model (1971). Longitudinal mild bars are modeled using “Steel02”, based on the Giuffre-Menegotto-Pinto model.

The prestressing strands are modeled separately from the beam-column fiber section by using truss elements fixed at the bottom and connected rigidly to the fiber section at the top. As no yielding of the strands occurred during the tests, the stress-strain relationship of the truss element is assumed to be linear. Rigid element connects the specimen fiber section to the anchorage of the prestressing strands, which are modeled by beam-column element with much higher strength and stiffness.

4.1.2 Longitudinal bar slip deformation

Longitudinal bar slip deformation results from the extension of the mild longitudinal bar from the specimen footing, this deformation generates rigid body rotation of the specimen that can substantially increase member flexibility (Ghannoum and Moehle 2012). To model bar slip deformation, a zero length fiber section element is used. The section of the element has the same geometry as the fiber section of the beam-column element it is attached to but with different

material properties for its steel and concrete fibers (Ghannoum 2007; Melo et al. 2011; Ghannoum and Moehle 2012; Zhang et al. 2013).

For steel fiber in the fiber section element, the constitutive law of the steel reinforcement is modified from a stress-strain relation to a stress-slip relation. A hysteretic model for the bar stress versus loaded-end slip response developed by Zhao and Sritharan (2007) is adopted, and the bar stress σ versus loaded-end slip s relationship is shown in Fig. 13. The slip values corresponding to bar yielding (s_y) and ultimate strength (s_u) are calculated using Eqs. (10) and (11), respectively.

$$s_y(\text{mm}) = 2.54\left(\frac{d_b(\text{mm})}{8437}\frac{f_y(\text{MPa})}{\sqrt{f_c^{'}}(\text{MPa})}(2\alpha+1)\right)^{1/\alpha} + 0.34 \tag{10}$$

$$s_u(\text{mm}) = (30 \sim 40)s_y \tag{11}$$

where, d_b is the bar diameter, α is the parameter used in the local bond-slip relation and is taken as 0.4.

For parameters shown in Fig. 13, f_u is the ultimate strength of the mild reinforcing bar. K is the slope of the straight line for bar stress σ versus loaded-end slip s relationship, and b is stiffness reduction factor (b=0.3～0.5). R is power index of unloading/reloading curve (R=0.5～1.0).

For concrete fiber in the fiber section element, the “Concrete01” uniaxial material model is also used as in the beam-column element. While the concrete strain at maximum stress is multiplied by a scale factor F_{conc} (F_{conc}=10～20) to maintain compatibility between the beam-column element and the bar slip section element (Ghannoum, 2007), as shown in Fig. 14.

4.2 Comparison between numerical and experimental results

It is very difficult to model the residual concrete crack width for reinforced concrete structures. Only the hysteretic curves, residual drifts and prestressing strand stress are compared with the test results in this study.

In Fig. 15, a comparison between experimental and numerical hysteretic curves of the specimens is illustrated. It can be seen that the calculated curves of all the specimens coincide well with experimental results in terms of strength, stiffness, residual displacement and overall performance. These results indicate that the proposed numerical model is adequate to evaluate the hysteretic behavior of the pier specimens with unbonded prestressing strands.

Figure 16 shows the residual drifts of the specimens from experimental results and numerical analyses. In general, a good agreement is observed between the numerical and experimental results. For specimens PRC-1, PRC-3, and PRC-6, the simulated residual drifts are slightly larger than the corresponding experimental results in the negative direction. But more accurate numerical results are observed in the positive direction. The differences between the experimental and numerical results are very likely caused by the asymmetry of the specimen response during the tests.

Taken strand PS-2 (for specimen PRC-6, PS is taken since the stress was measured together as mentioned above) as an example, Figure 17 shows the strand stress of the specimens from experimental results and numerical analysis. It could be found that the simulated strand stress agree well with experimental results, which indicates that the proposed numerical model can accurately simulate the unbonded strand stress under cyclic loading.

5 Conclusions

Longitudinal unbonded prestressing strands are used to minimize the residual drift and residual concrete crack width in RC bridge piers. A series of experimental studies were carried out to examine the influences of various parameters including the prestressing force ratio, the mechanical pretressing ratio and the location of the prestressing strands on the bridge pier residual drift and residual concrete crack width. A FE model was developed and calibrated by using the open-source finite element code OpenSees. Following conclusions are drawn:

1. During the tests, no obvious difference is observed for the damage development and failure pattern between the specimens with and without prestressing strands. Flexural failure occurs in all the specimens under lateral cyclic loading, and these failures include concrete cracking, concrete cover spalling and longitudinal bar buckling.

2. The residual drift of bridge piers can be reduced by using the vertical unbonded prestressing strands, and the mechanical prestressing ratio is an important parameter for controlling the residual drift of the piers. Larger mechanical prestressing ratio would lead to smaller residual drift. The initial prestressing stress and the arrangement of the strands have little influence on residual drift of the piers.

3. The residual concrete crack width of the piers can be reduced significantly by using vertical unbonded prestressing strands. Both the prestressing force ratio and the mechanical prestressing ratio have a significant influence on the residual crack width, larger prestressing force ratio and mechanical prestressing ratio would lead to smaller residual crack width. The arrangement of the strands has little influence on the residual crack width.

4. During the tests, the strand stress increases or decreases almost linearly with the pier drift. Except for one strand fails due to damage of the anchorage, all the other strands are elastic and no yielding or rupturing damage is observed. To minimize the residual drift and concrete crack width in bridge piers, the strand should be kept effective under seismic actions.

5. The lateral strength of the pier specimens can be increased by using unbonded prestressing strands, while the ductility capacity of the piers with prestressing strands is not obviously changed. It is practical to reduce the seismic residual drift and residual concrete crack width of bridge piers by using prestressing strands for commonly used bridge piers with an axial load ratio less than 0.1.

6. The proposed numerical model is adequate to evaluate the hysteretic behavior of the pier specimens with prestressing strands.

Acknowledgements

The authors gratefully acknowledge the support for this research by the National Natural Science Foundation of China under Grant Nos. 51008041 and 51178071, China Postdoctoral Science Foundation under Grant Nos. 2013M540226 and 2014T70250. The third author acknowledges the partial support from Australian Research Council Discovery Early Career Research Award (DECRA).

References

Bentz E C (2000) Sectional analysis of reinforced concrete members. Ph.D. Thesis, University of Toronto, Toronto, Canada

Bentz E C, Vecchio F J, Collins M P (2006) Simplified modified compression field theory for calculating shear strength of reinforced concrete elements. ACI Structural Journal 103(4): 614-624

Fujino Y, Hashimoto S, Abe M (2005) Damage analysis of Hanshin expressway viaducts during 1995 Kobe earthquake. I: Residual inclination of reinforced concrete piers. Journal of Bridge Engineering, ASCE 10(1): 45-53

Ghannoum W M (2007) Experimental and analytical dynamic collapse study of a reinforced concrete frame with light transverse reinforced. Ph.D. Thesis, University of California, Berkeley, Berkeley, USA

Ghannoum W M, Moehle J P (2012) Dynamic collapse analysis of a concrete frame sustaining column axial failures. ACI Structural Journal 109(3): 403-412

Guo A X, Yuan W, Lan C M, Guan X C, Li H (2015) Time-dependent seismic demand and fragility of deteriorating bridges for their residual service life. Bulletin of Earthquake Engineering 13(8): 2389-2409.

Hashimoto S, Fujino Y, Abe M (2005) Damage analysis of Hanshin expressway viaducts during 1995 Kobe earthquake. II: Damage mode of single reinforced concrete piers. Journal of Bridge Engineering, ASCE 10(1): 54-60

Iemura H, Takahashi Y, Sogabe N (2004) Development of unbonded bar reinforced concrete structures. Proceeding of the 13th World Conference on Earthquake Engineering, Vancouver, B.C., Canada, Paper Number: 1537

Kawashima K, Macrae G A, Hoshikuma J I, Nagaya K (1998) Residual displacement response spectrum. Journal of Structural Engineering, ASCE 124(5): 523-530

Kent D C, Park R (1971) Flexural members with confined concrete. Journal of the Structural Division 97(7): 1969-1990

Mahin S, Sakai J, Jeong H (2006) Use of partially prestressed reinforced concrete columns to reduce post-earthquake residual displacements of bridges. Proceeding of the 5th National Seismic Conference on Bridge & Highways, San Francisco, America

Mazzoni S, Mckenna F, Scott M H, Fenves G L (2007) Opensees command language manual. Pacific Earthquake Engineering Research Center, University of California, Berkeley

Melo J, Fernandes C, Varum H, Rodrigues H, Costa A, Arêde A (2011) Numerical modeling of the cyclic behavior of RC elements built with plain reinforcing bars. Engineering Structures 33: 273-286

Moshref A, Tehranizadeh M, Khanmohammadi M (2015) Investigation of the reliability of nonlinear modeling approaches to capture the residual displacements of RC columns under seismic loading. Bulletin of Earthquake Engineering 13(8): 2327-2345.

Ou Y C, Wang P H, Tsai M S, Chang K C, Lee G C (2010) Large-scale experimental study of precast segmental unbonded posttensioned concrete bridge columns for seismic regions. Journal of Structural Engineering, ASCE 136(3): 255-264

Sakai J, Mahin S A (2004a) Analytical investigations of new methods for reducing residual displacements of reinforced concrete bridge columns. Report No. PEER-2004/02, Pacific Earthquake Engineering Research Center, College of Engineering, University of California, Berkeley, California, USA.

Sakai J, Mahin S A (2004b) Mitigation of residual displacements of circular reinforced concrete bridge columns. Proceeding of the 13th World Conference on Earthquake Engineering, Vancouver, B.C., Canada, Paper Number: 1622

Shim C S, Chung C H, Kim H H (2008) Experimental evaluation of seismic performance of precast segmental bridge piers with a circular solid section. Engineering Structures 30: 3782-3792

Shoraka M B, Elwood K J (2013) Mechanical model for non ductile reinforced concrete columns. Journal of Earthquake Engineering 17(7): 937-957

Spacone E, Filippou F C, Taucer F F (1996a) Fiber beam-column model for non-linear analysis of R/C frames: Part I. Formulation. Earthquake Engineering and Structural Dynamics 25(7): 711-725

Spacone E, Filippou F C, Taucer F F (1996b) Fiber beam-column model for non-linear analysis of R/C frames: Part II. Applications. Earthquake Engineering and Structural Dynamics 25(7): 727-742

Sun Z, Wang D, Guo X, Si B, Huo Y (2012) Lessons learned from the damaged Huilan interchange in the 2008 Wenchuan earthquake. Journal of Bridge Engineering, ASCE 17(1): 15-24

Wang J C, Ou Y C, Chang K C, Lee G C (2008) Large-scale seismic tests of tall concrete bridge columns with precast segmental construction. Earthquake Engineering and Structural Dynamics 37(12): 1449-1465

Yamashita R, Sanders D H (2009) Seismic performance of precast unbonded prestressed concrete columns. ACI Structural Journal 106(6): 821-830

Yavari S, Elwood K J, Wu C L (2009) Collapse of a nonductile concrete frame: Evaluation of analytical models. Earthquake Engineering and Structural Dynamics 38(2): 225-241

Zatar W A, Mutsuyoshi H (2002) Residual displacements of concrete bridge piers subjected to near field earthquakes. ACI Structural Journal 99(6): 740-749

Zhang Y Y, Harries K A, Yuan W C (2013) Experimental and numerical investigation of the seismic performance of hollow rectangular bridge piers constructed with and without steel fiber reinforced concrete. Engineering Structures 48: 255-265

Zhao J, Sritharan S (2007) Modeling of strain penetration effects in fiber-based analysis of reinforced concrete structures. ACI Structural Journal 104(2): 133-141

Zhuang W L, Liu Z Y, Jiang J S (2009) Earthquake-induced damage analysis of highway bridges in Wenchuan earthquake and countermeasures. Chinese Journal of Rock Mechanics and Engineering 28(7): 1377-1387. [in Chinese]

List of table captions

Table 1 Test parameters of the pier specimens

Table 2 The experimental and theoretical concrete cracking strengths of the specimens

Table 3 The strand stress of the specimens

Table 4 Strength and ductility parameters of the specimens

Table 1 Test parameters of the pier specimens

Specimen	Longitudinal bars	Prestressing strands	n	η	ζ	λ	Description of the specimen
RC-1	Eight 12 mm-dia. bars	Without	0.1	0.1	0	0	Specimen without prestressing strands
PRC-1	Eight 12 mm-dia. bars	Four 12.7 mm-dia. strands	0.2	0.1	0.1	0.61	Standard specimen with prestressing strands
PRC-2	Eight 8 mm-dia. bars	Four 12.7 mm-dia. strands	0.2	0.1	0.1	0.76	Longitudinal bars were reduced compared with specimen PRC-1
PRC-3	Eight 12 mm-dia. bars	Two 12.7 mm-dia. strands	0.15	0.1	0.05	0.44	Prestressing strands were reduced compared with specimen PRC-1
PRC-4	Eight 12 mm-dia. bars	Four 12.7 mm-dia. strands	0.15	0.1	0.05	0.61	Initial prestressing stress was reduced compared with specimen PRC-1
PRC-5	Eight 12 mm-Dia. bars	Four 12.7 mm-dia. strands	0.25	0.1	0.15	0.61	Initial prestressing stress increased compared with specimen PRC-1
PRC-6	Eight 12 mm-dia. bars	Four 12.7 mm-dia. strands	0.2	0.1	0.1	0.61	Concentrated prestressing strands was used

Table 2 The experimental and theoretical concrete cracking strengths of the specimens

Specimen	$F_{cr,e}$ (kN)	$F_{cr,t}$ (kN)	$F_{cr,e}/F_{cr,t}$
RC-1	20	17	1.2
PRC-1	34	34	1.0
PRC-2	26	33	0.8
PRC-3	24	30	0.8
PRC-4	29	24	1.2
PRC-5	31	39	0.8
PRC-6	24	30	0.8

635 **Table 3 The strand stress of the specimens**

Specimen	Strand	$\sigma_{PS,1}$ (MPa)	$\sigma_{PS,max}$ (MPa)	$\sigma_{PS,min}$ (MPa)	$\sigma_{PS,var}$ (MPa)	
					$\sigma_{PS,max}$-$\sigma_{PS,1}$	$\sigma_{PS,1}$-$\sigma_{PS,min}$
PRC-1	PS1	686	1020	573	334	113
	PS2	662	1057	464	395	198
	PS3	660	1061	502	401	158
	PS4	656	998	520	342	136
PRC-2	PS1	714	998	605	284	109
	PS2	766	1031	640	265	126
	PS3*	743	786	700	43	43
	PS4	694	1098	500	404	194
PRC-3	PS1	773	1173	427	400	346
	PS2	816	1246	619	430	197
PRC-4	PS1	310	521	8	211	302
	PS2	342	644	197	302	145
	PS3	326	606	42	280	284
	PS4	320	673	128	353	192
PRC-5	PS1	925	1212	732	287	193
	PS2	1037	1289	857	252	180
	PS3	1097	1410	931	313	166
	PS4	1036	1342	845	306	191
PRC-6	PS	701	855	694	154	7

636 * Strand failed as a result of damage of the anchorage at 0.5% drift.

637

638

639 **Table 4 Strength and ductility parameters of the specimens**

Specimens	F_{max} (kN)	Δ_1 (mm)	Δ_μ (mm)	μ_Δ	R (%)
RC-1	70.9	7.0	35.3	5.0	3.2
PRC-1	95.3	8.0	37.2	4.7	3.4
PRC-2	81.5	6.0	31.7	5.3	2.9
PRC-3	83.8	7.6	38.7	5.1	3.5
PRC-4	84.7	8.0	38.3	4.8	3.5
PRC-5	102.3	7.7	32.6	4.2	3.0
PRC-6	93.5	7.5	36.8	4.9	3.3

640

641

642

643

644

645

646

647

648

649

650

651

652

653

654

655

List of Figure Captions

Fig. 1 Design details of the pier specimens: **a** elevation view; **b** reinforcement layout; **c** prestressing strand layout (unit: mm)

Fig. 2 Test setup

Fig. 3 Lateral loading histories

Fig. 4 Failure patterns of the specimens: **a** failure pattern of the specimen without prestressing strands at the end of the test (RC-1); **b** failure pattern of a specimen with prestressing strands at the end of the test (PRC-1); **c** flexural and shear concrete cracks; **d** concrete cover spalling and exposing of the transverse bars; **e** longitudinal bar buckling and concrete core crushing damage

Fig. 5 Sketches of concrete spalling heights of specimens: **a** RC-1; **b** PRC-1; **c** PRC-2; **d** PRC-3; **e** PRC-4; **f** PRC-5; **g** PRC-6

Fig. 6 Hysteretic curves of the specimens: **a** RC-1; **b** PRC-1; **c** PRC-2; **d** PRC-3; **e** PRC-4; **f** PRC-5; **g** PRC-6

Fig. 7 Strand tress-drift relationship of the specimens: **a** PRC-1; **b** PRC-2; **c** PRC-3; **d** PRC-4; e PRC-5; **f** PRC-6

Fig. 8 Prestressing force-drift relationship of the specimens

Fig. 9 Residual drifts: **a** all the specimens; **b** RC-1, PRC-1 and PRC-2; **c** RC-1, PRC-1 and PRC-3; **d** RC-1, PRC-1 and PRC-4; **e** RC-1, PRC-1 and PRC-5; **f** RC-1, PRC-1 and PRC-6

Fig. 10 Residual concrete crack widths: **a** all the specimens; **b** RC-1, PRC-1 and PRC-2; **c** RC-1, PRC-1 and PRC-3; **d** RC-1, PRC-1 and PRC-4; **e** RC-1, PRC-1 and PRC-5; **f** RC-1, PRC-1 and PRC-6

Fig. 11 Definition of the strength and ductility parameters

Fig. 12 Numerical model of the specimens

Fig. 13 Bar stress versus loaded-end slip response model proposed by Zhao and Sritharan [20]: **a** under monotonic loading; **b** hysteretic response

Fig. 14 Stress strain relations for beam-column element and bar slip element concrete fibers

Fig. 15 Experimental and numerical hysteretic curves: **a** RC-1; **b** PRC-1; **c** PRC-2; **d** PRC-3; **e** PRC-4; **f** PRC-5; **g** PRC-6

Fig. 16 Experimental and numerical residual drifts: **a** RC-1; **b** PRC-1; **c** PRC-2; **d** PRC-3; **e** PRC-4; **f** PRC-5; **g** PRC-6

Fig. 17 Experimental and numerical strand stress: **a** PRC-1; **b** PRC-2; **c** PRC-3; **d** PRC-4; **e** PRC-5; **f** PRC-6

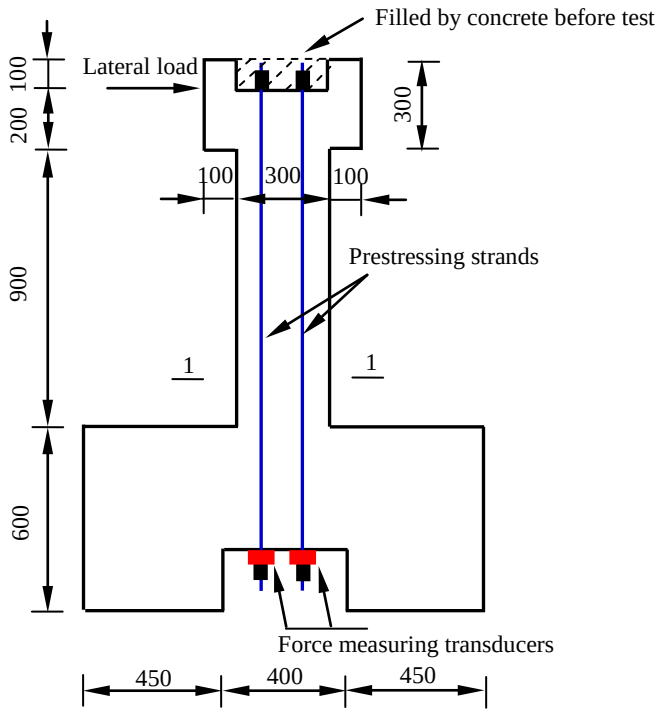
Filled by concrete before test
Lateral load
100
200
300
100
300
100
Prestressing strands
900
1
1
600
Force measuring transducers
450
400
450

(a)

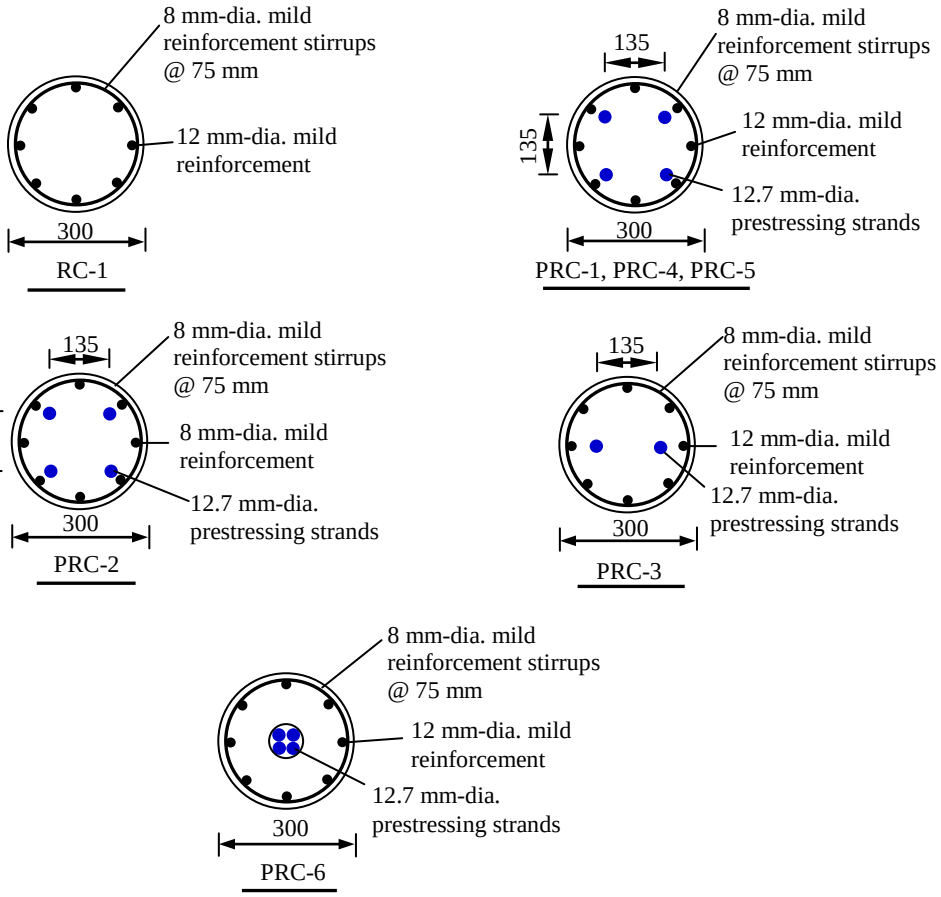
8 mm-dia. mild reinforcement stirrups @ 75 mm
12 mm-dia. mild reinforcement
300
RC-1
135
8 mm-dia. mild reinforcement stirrups @ 75 mm
135
12 mm-dia. mild reinforcement
12.7 mm-dia. prestressing strands
300
PRC-1, PRC-4, PRC-5
135
8 mm-dia. mild reinforcement stirrups @ 75 mm
135
8 mm-dia. mild reinforcement
12.7 mm-dia. prestressing strands
300
PRC-2
135
8 mm-dia. mild reinforcement stirrups @ 75 mm
12 mm-dia. mild reinforcement
12.7 mm-dia. prestressing strands
300
PRC-3
8 mm-dia. mild reinforcement stirrups @ 75 mm
12 mm-dia. mild reinforcement
12.7 mm-dia. prestressing strands
300
PRC-6

(b)

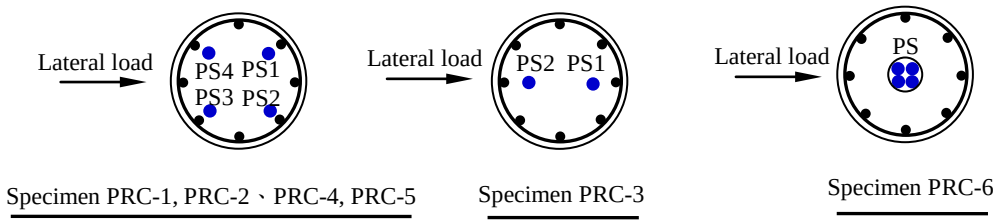

(c)

Fig. 1 Design details of the pier specimens: **a** elevation view; **b** reinforcement layout; **c** prestressing strand layout (unit: mm)

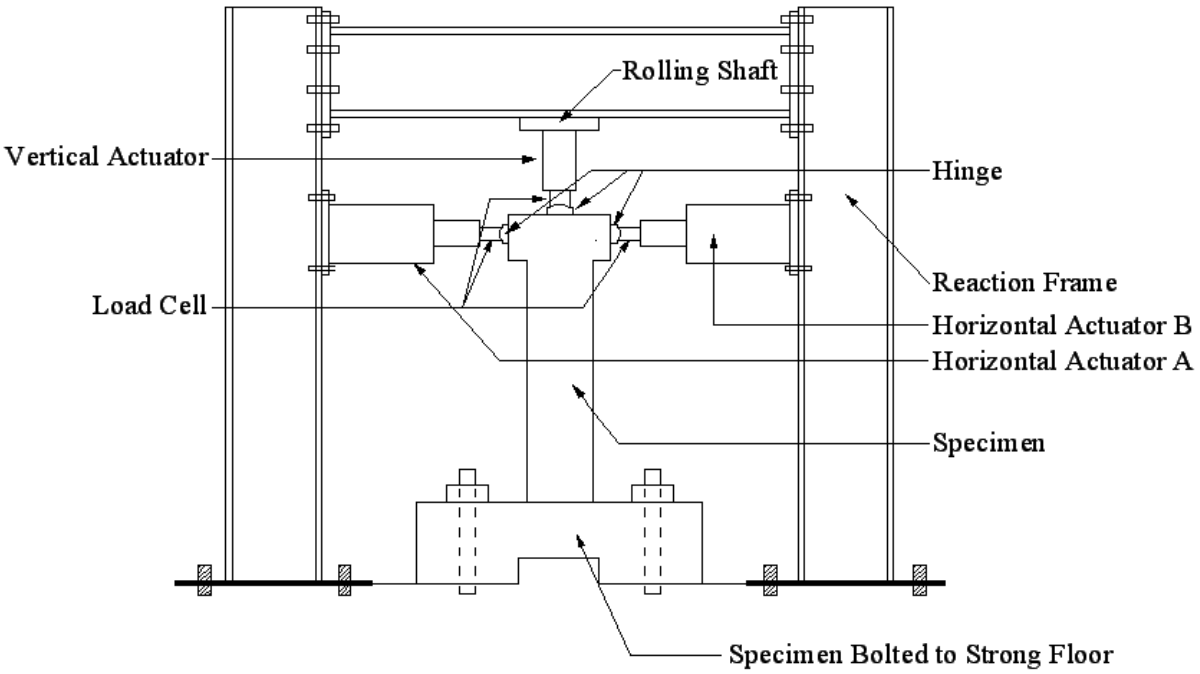

760

761 **Fig. 2** Test setup

762

763

764

765

766

767

768

769

770

771

772

773

774

775

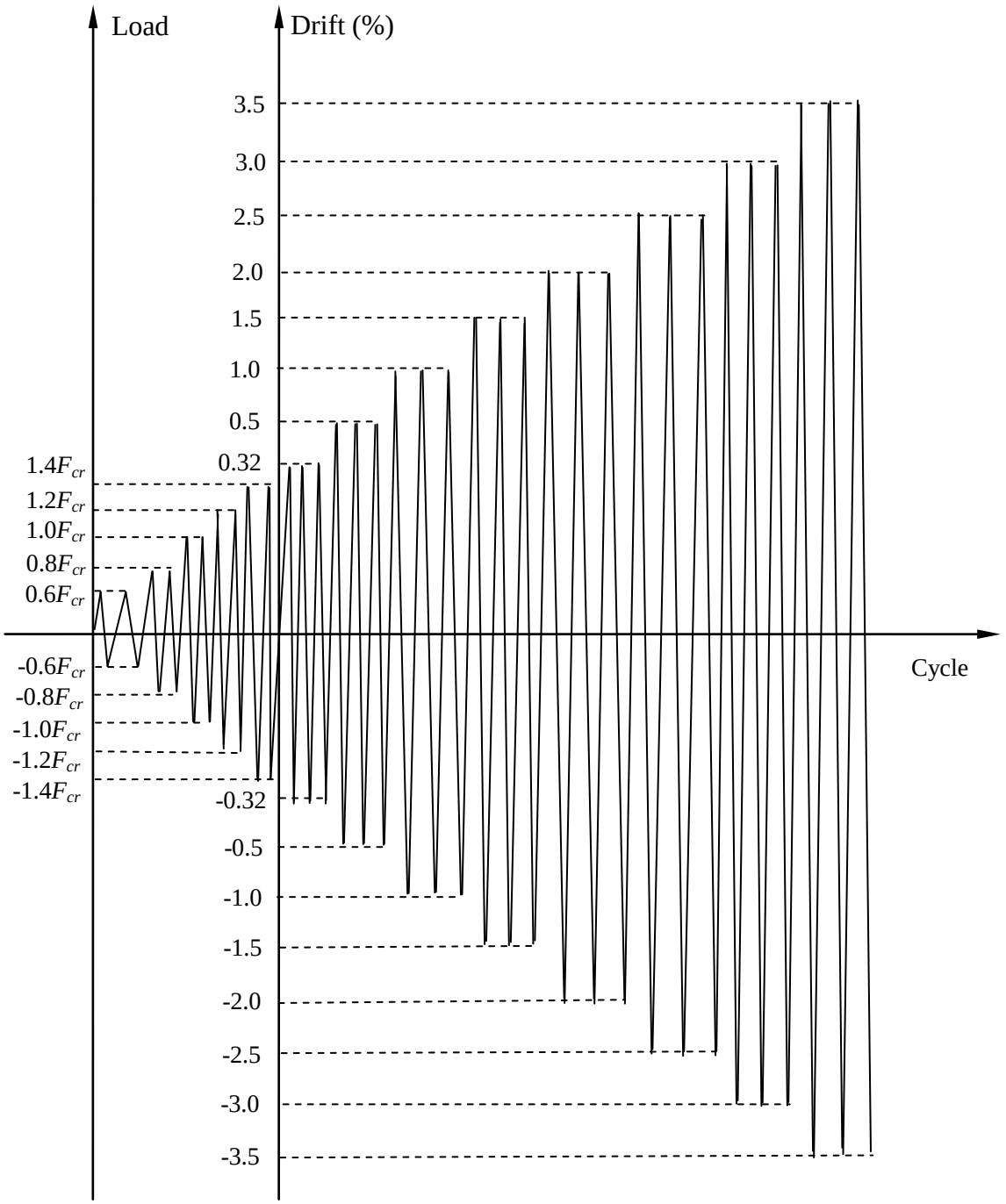

Fig. 3 Lateral loading histories

(a) (b) (c)

(d) (e)

Fig. 4 Failure patterns of the specimens: **a** failure pattern of the specimen without prestressing strands at the end of the test (RC-1); **b** failure pattern of a specimen with prestressing strands at the end of the test (PRC-1); **c** flexural and shear concrete cracks; **d** concrete cover spalling and exposing of the transverse bars; **e** longitudinal bar buckling and concrete core crushing damage

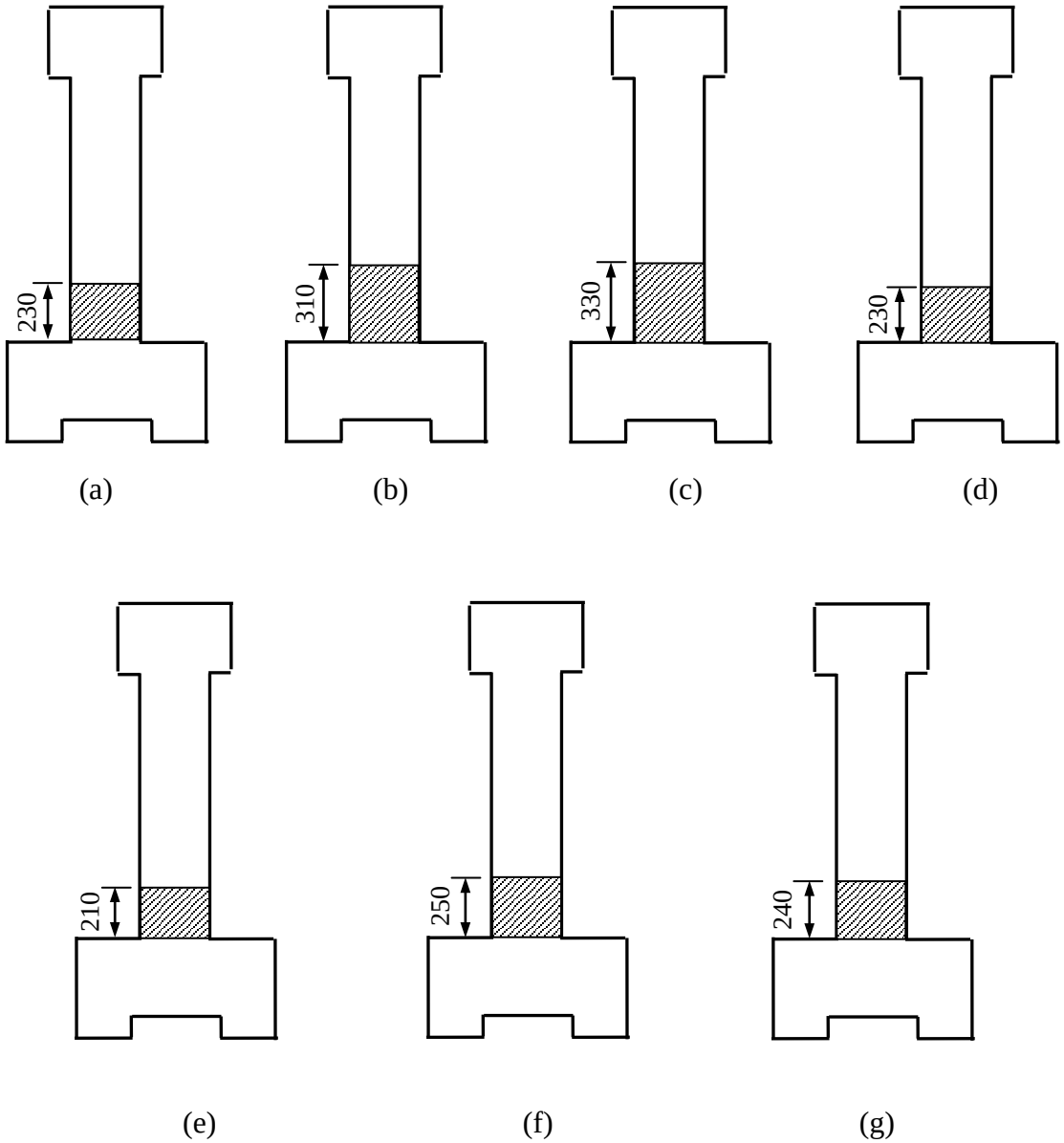

Fig. 5 Sketches of concrete spalling heights of specimens: **a** RC-1; **b** PRC-1; **c** PRC-2; **d** PRC-3; **e** PRC-4; **f** PRC-5; **g** PRC-6

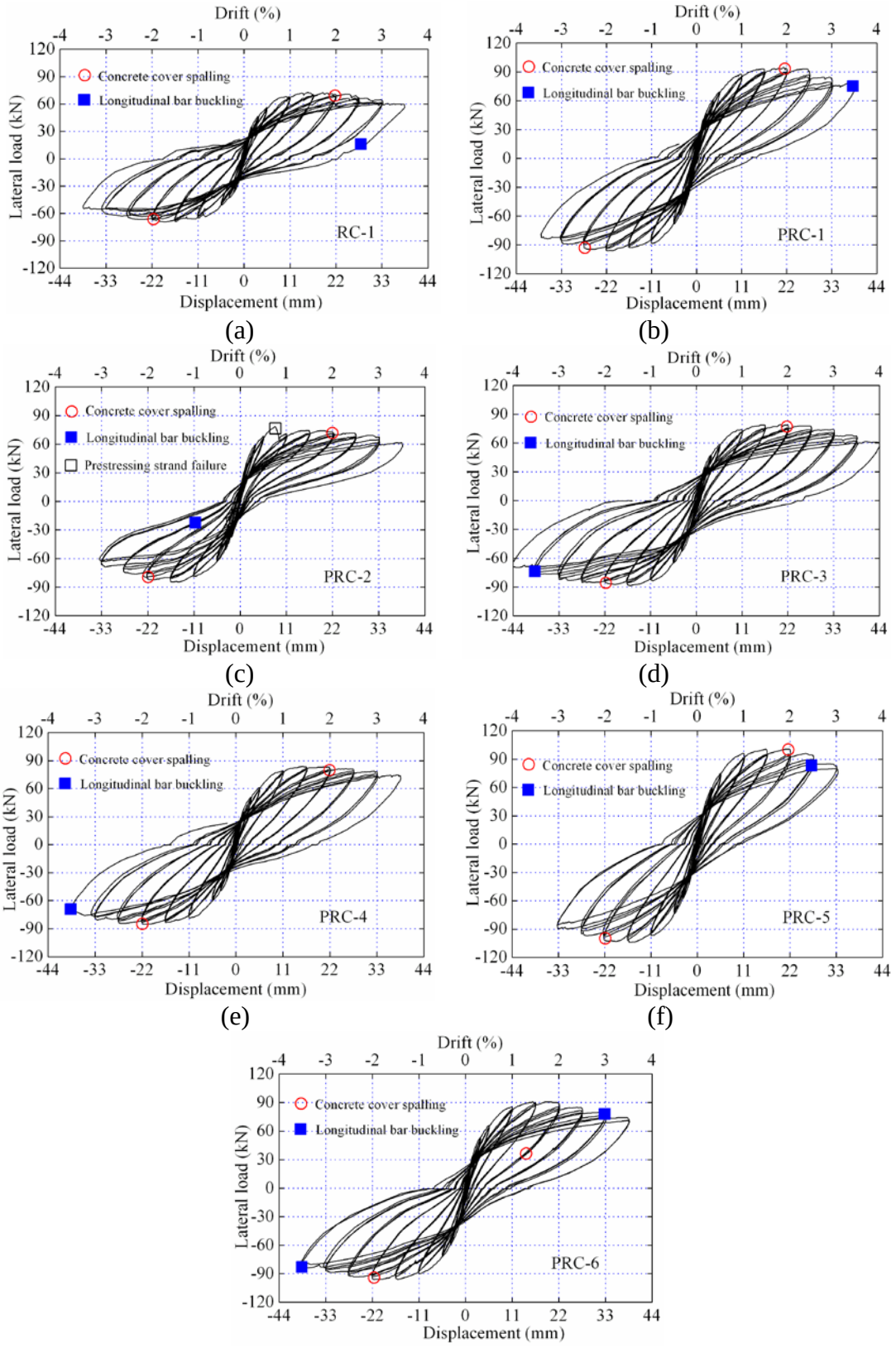

Fig. 6 Hysteretic curves of the specimens: **a** RC-1; **b** PRC-1; **c** PRC-2; **d** PRC-3; **e** PRC-4; **f** PRC-5; **g** PRC-6

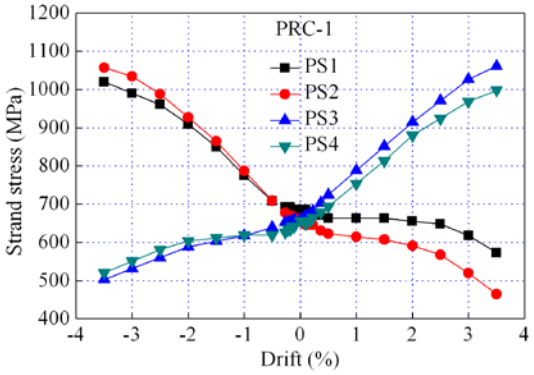

(a)

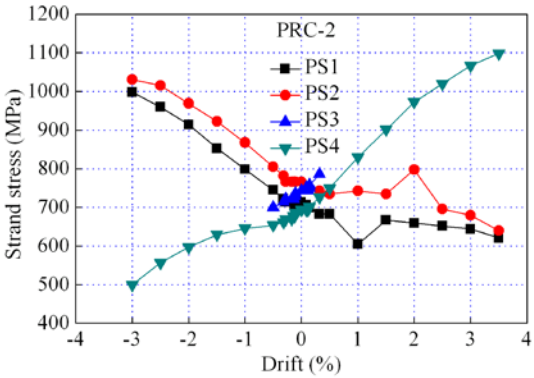

(b)

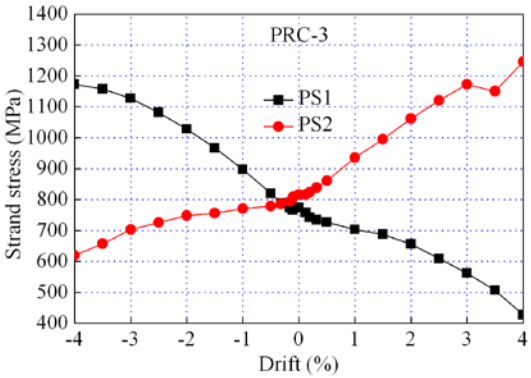

(c)

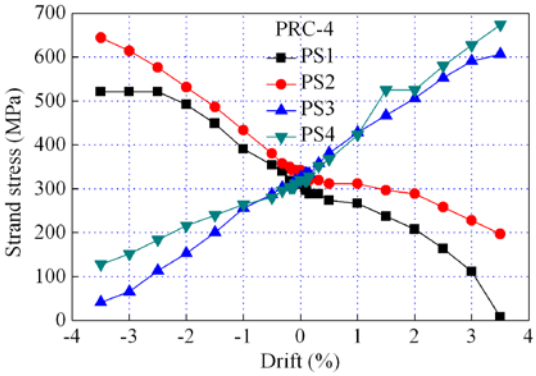

(d)

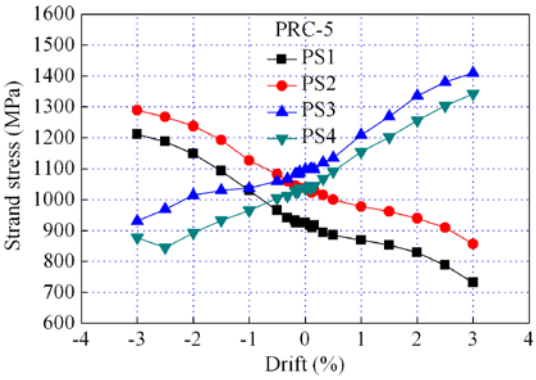

(e)

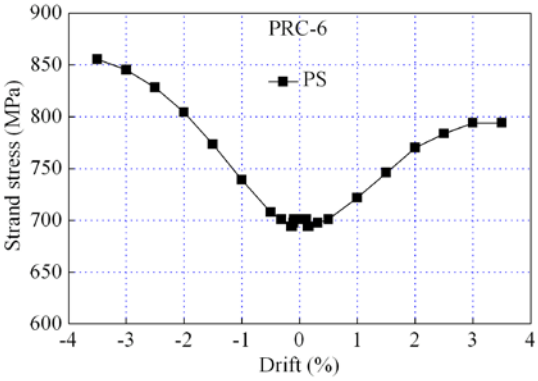

(f)

Fig. 7 Strand tress-drift relationship of the specimens: **a** PRC-1; **b** PRC-2; **c** PRC-3; **d** PRC-4; e PRC-5; **f** PRC-6

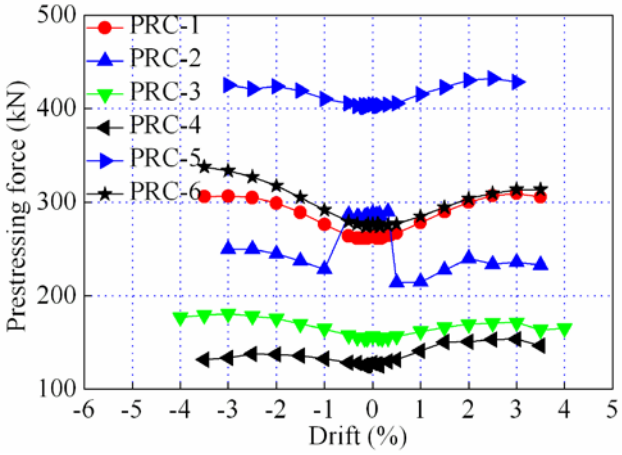

Fig. 8 Prestressing force-drift relationship of the specimens

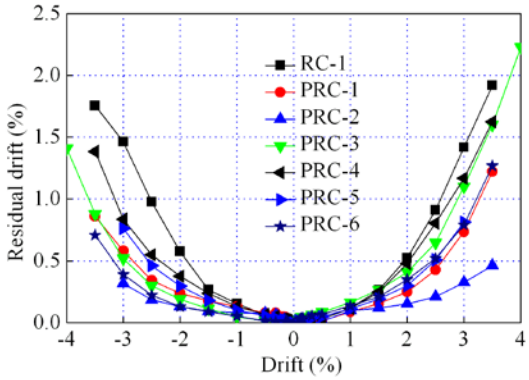

(a)

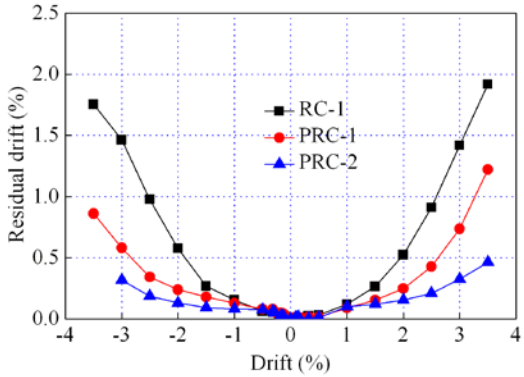

(b)

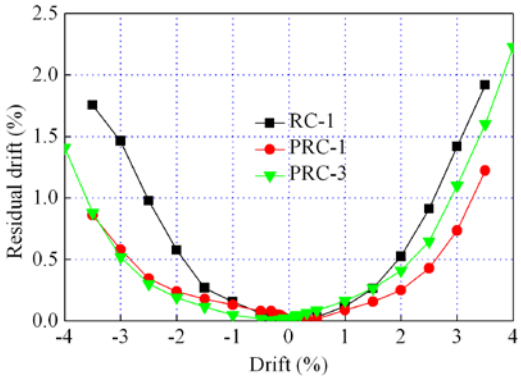

(c)

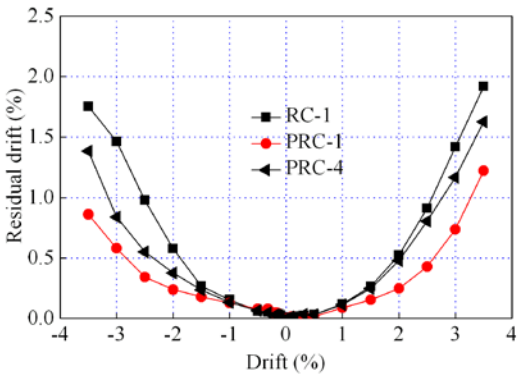

(d)

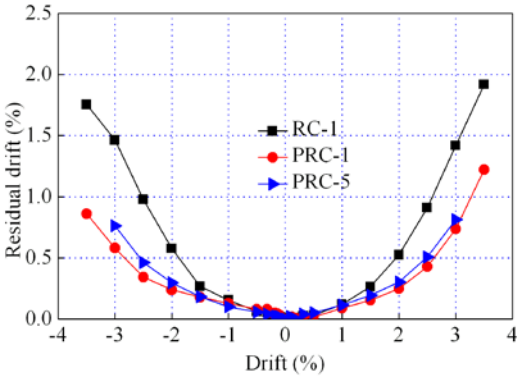

(e)

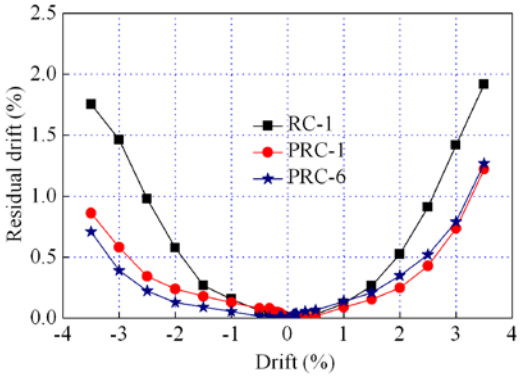

(f)

Fig. 9 Residual drifts: **a** all the specimens; **b** RC-1, PRC-1 and PRC-2; **c** RC-1, PRC-1 and PRC-3; **d** RC-1, PRC-1 and PRC-4; **e** RC-1, PRC-1 and PRC-5; **f** RC-1, PRC-1 and PRC-6

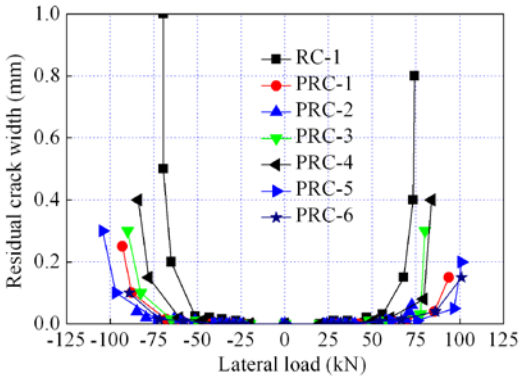

(a)

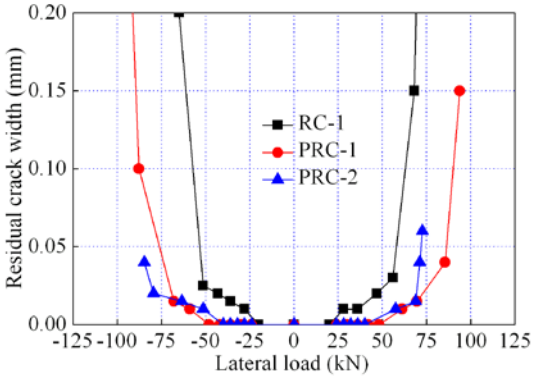

(b)

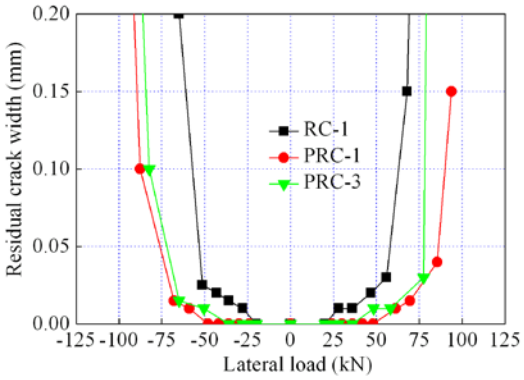

(c)

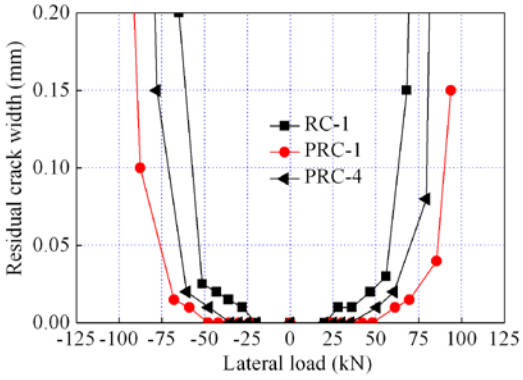

(d)

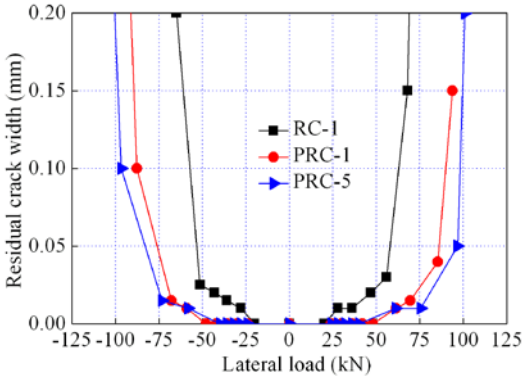

(e)

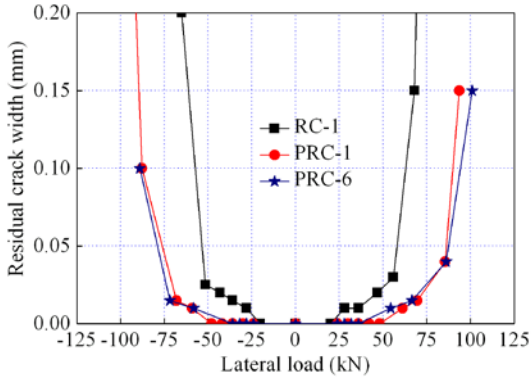

(f)

Fig. 10 Residual concrete crack widths: **a** all the specimens; **b** RC-1, PRC-1 and PRC-2; **c** RC-1, PRC-1 and PRC-3; **d** RC-1, PRC-1 and PRC-4; **e** RC-1, PRC-1 and PRC-5; **f** RC-1, PRC-1 and PRC-6

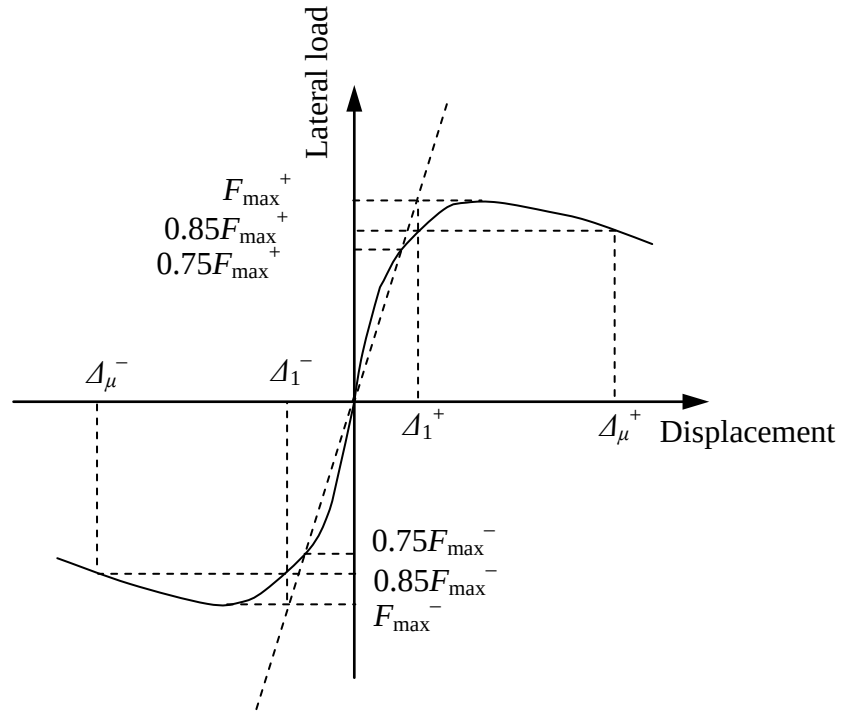

Fig. 11 Definition of the strength and ductility parameters

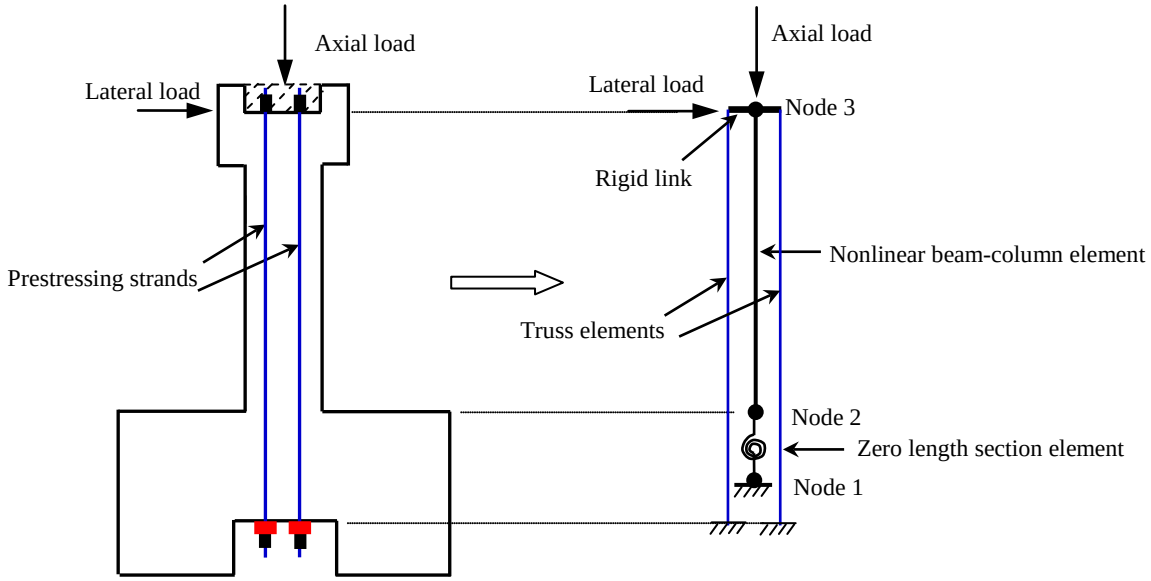

Fig. 12 Numerical model of the specimens

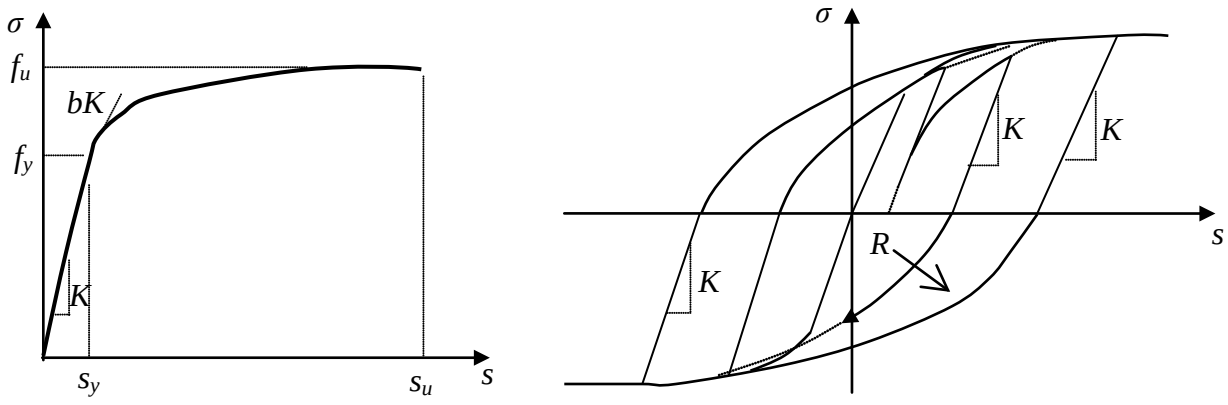

(a) (b)

Fig. 13 Bar stress versus loaded-end slip response model proposed by Zhao and Sritharan [20]: **a** under monotonic loading; **b** hysteretic response

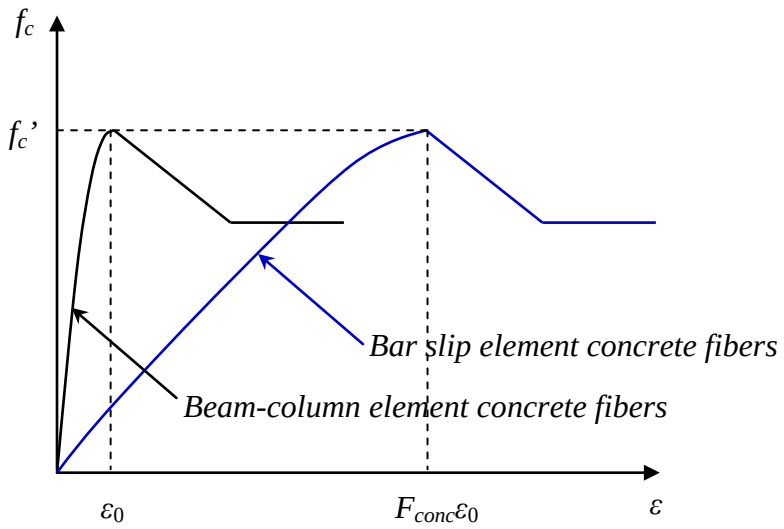

Fig. 14 Stress strain relations for beam-column element and bar slip element concrete fibers

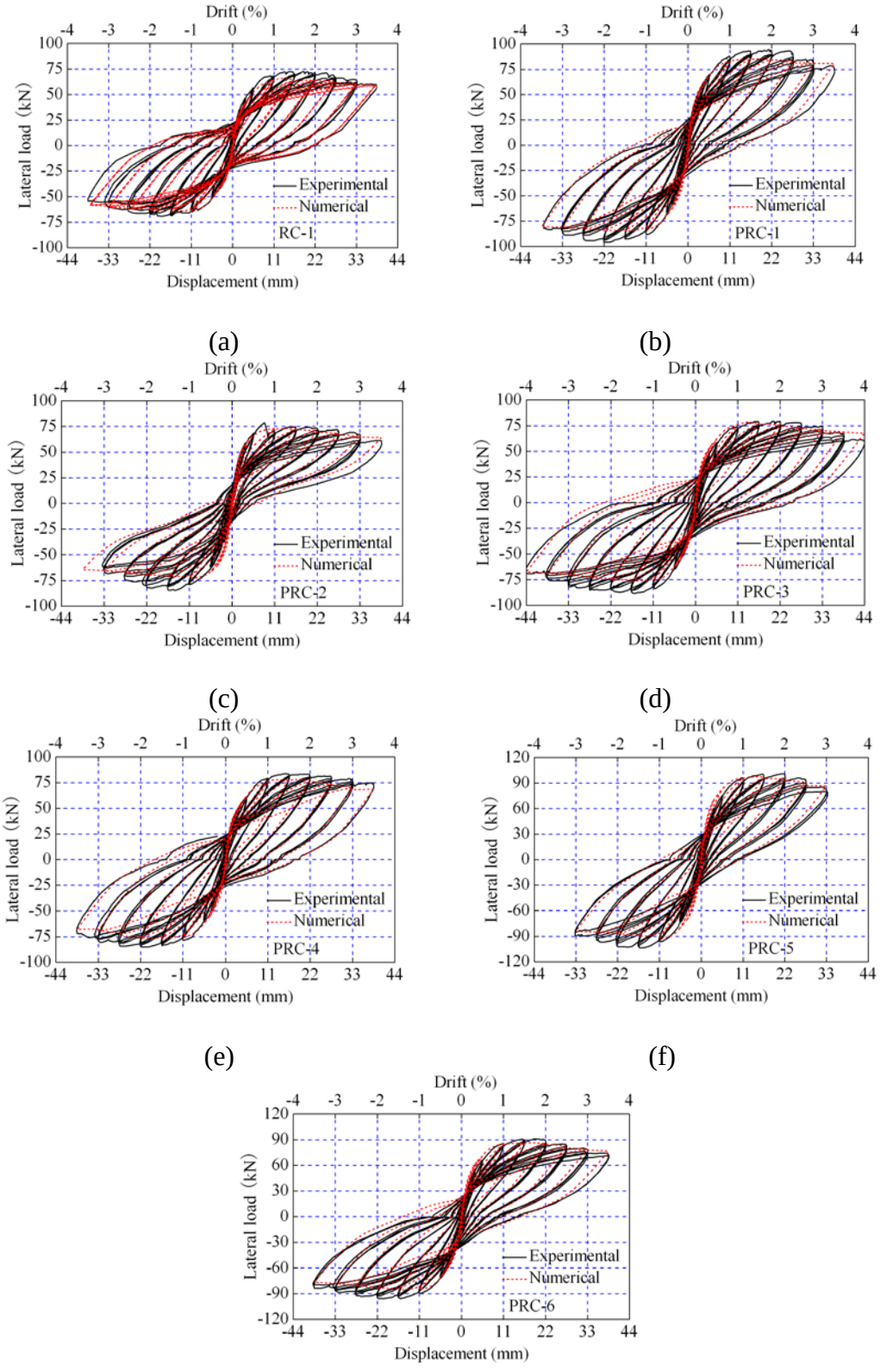

Fig. 15 Experimental and numerical hysteretic curves: **a** RC-1; **b** PRC-1; **c** PRC-2; **d** PRC-3; **e** PRC-4; **f** PRC-5; **g** PRC-6

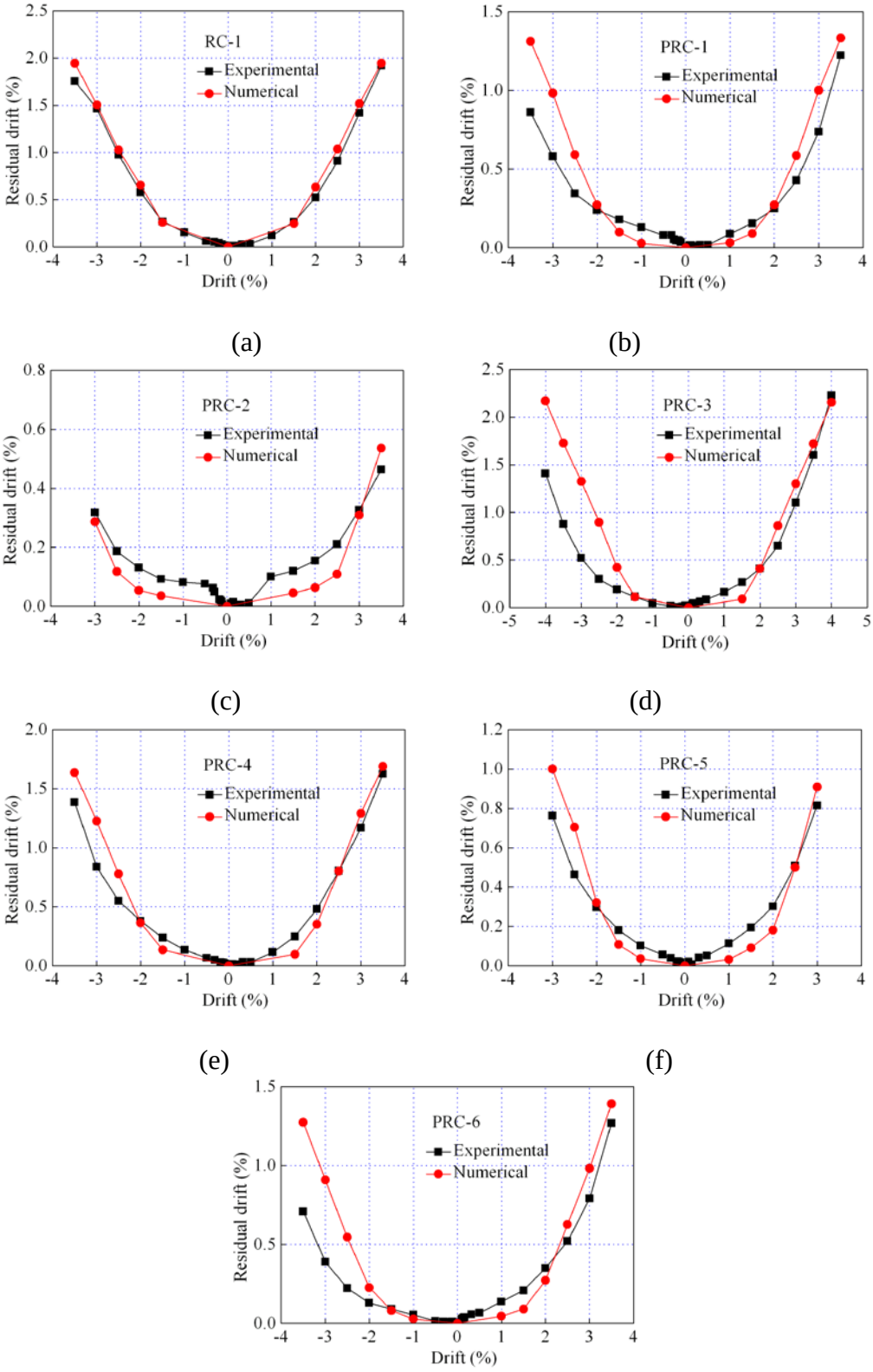

Fig. 16 Experimental and numerical residual drifts: **a** RC-1; **b** PRC-1; **c** PRC-2; **d** PRC-3; **e** PRC-4; **f** PRC-5; **g** PRC-6

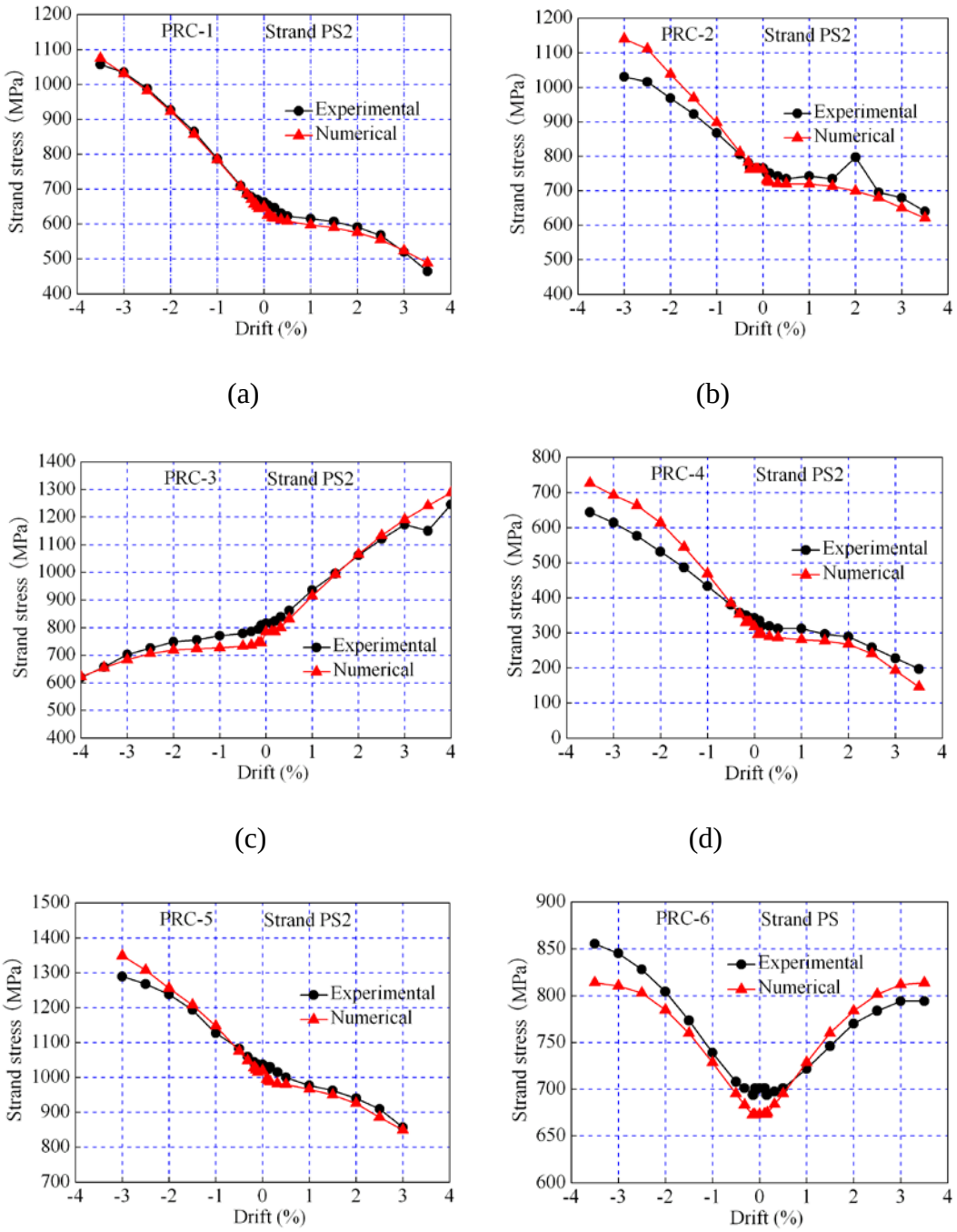

Fig. 17 Experimental and numerical strand stress: **a** PRC-1; **b** PRC-2; **c** PRC-3; **d** PRC-4; **e** PRC-5; **f** PRC-6